Journal of Ceramic Processing Research. Vol. 12, No. 3, pp. 314~318 (2011)

J O U R N A L O F
Ceramic Processing Research

Rapid consolidation of nanostuctured MgO –Mg_2SiO_4 composites by high frequency induction heated sintering

In-Jin Shon[a,*], In-Yong Ko[a], Hui-Soo Jun[a], Kyung-Tae Hong[b], Se-Hoon Oh[c], Jung-Mann Doh[b] and Jin-Kook Yoon[b]

[a]*Division of Advanced Materials Engineering and the Research Center of Advanced Materials Development, Engineering College, Chonbuk National University, 561-756, Republic of Korea*

[b]*Advanced Functional Materials Research Center, Korea Institute of Science and Technology, PO Box 131, Cheongryang, Seoul 130-650, Republic of Korea*

[c]*Department of Mechanical Engineering, Chung-Ang University, Seoul Korea 156-756, Korea*

The rapid sintering of nanostuctured MgO and MgO-Mg_2SiO_4 composites in a short time was investigated with a high-frequency induction heating sintering process. The advantage of this process is that it allows very quick densification to near theoretical density and prohibition of grain growth in nanostuctured materials. Highly dense nanostructured MgO and MgO-Mg_2SiO_4 composites were produced with simultaneous application of 80 MPa pressure and an induced current output of total power capacity (15 kW) within 2 minutes. The grain sizes of MgO and Mg_2SiO_4 in MgO, MgO-10 wt%SiO_2, MgO-20 wt%SiO_2, MgO-30 wt%SiO_2, and MgO-40 wt%SiO_2 sintered at 1400 °C and the hadnesses were investigated.

Key words: Sintering, MgO, Mg_2SiO_4, Nanostructured material, Powder metallurgy.

Introduction

In recent years, some Si and Mg containing ceramics have drawn interests in the development of bone implant materials [1-4]. Schwarz and Miline [5] have shown that silicon deficiency in rats results in skull deformation, with the cranial bones appearing flatter than normal. Magnesium is also undoubtedly one of the most important elements in the human body, and closely associated with mineralization of calcined tissues and indirectly influences mineral metabolism [6]. Mg_2SiO_4 has been reported as a new machinable biomaterial, and might be used in dental and orthopedic prostheses [7, 8]. Furthermore, Mg_2SiO_4 shows good refractoriness, with a melting point of 1890 °C, low thermal expansion, good chemical stability, and excellent insulation properties even at high temperature [9]. However, as in the case of many ceramic materials, the current concern about these materials focuses on their low fracture toughness below the ductile-brittle transition temperature [10]. To improve their mechanical properties, the approach commonly utilized has been the addition of a second phase to form composites and to make nanostructured materials. One example is the addition of MgO to Mg_2SiO_4 to improve the latter's properties. The attractive properties of MgO are high hardness, low density good corrosion and mechanical erosion resistance.

Nanocrystalline materials have received much attention as advanced engineering materials with improved physical and mechanical properties [11, 12]. In recent days, nanocrystalline powders have been developed by the thermochemical and thermomechanical process named the spray conversion process (SCP), co-precipitation and high energy milling [13-15]. However, the grain size in sintered materials becomes much larger than that in the pre-sintered powders due to the rapid grain growth during a conventional sintering process. Therefore, even though the initial particle size is less than 100 nm, the grain size increases rapidly up to 2 μm or larger during conventional sintering [16]. So, controlling grain growth during sintering is one of the keys to the commercial success of nanostructured materials. In this regard, the high frequency induction heated sintering method (HFIHS) which can make dense materials within 2 minutes has been shown to be effective in achieving this goal [17-20].

In this study, we investigated the sintering of MgO-Mg_2SiO_4 composites by the HFIHS method. The goal of this research is to produce dense nanostructured MgO-Mg_2SiO_4 materials.

Experimental Procedure

MgO powder with a grain size of < 45 μm and 99% purity and amorphous SiO_2 powder with a grain size of < 45 μm and 99.8% purity used in this research were supplied by Alfa. The powders(MgO, MgO-10 wt%SiO_2, MgO-20 wt%SiO_2, MgO-30 wt%SiO_2, MgO-40 wt%SiO_2) were first milled in a high-energy ball mill (Pulverisette-5 planetary mill) at 250 rpm for 4 h. Tungsten carbide balls (9 mm in diameter) were used in a sealed cylindrical

*Corresponding author:
Tel : +82-63-270-2381
Fax: +82-63-270-2386
E-mail: ijshon@chonbuk.ac.kr

stainless steel vial under an argon atmosphere. The weight ratio of balls-to-powder was 30 : 1. Milling resulted in a significant reduction of the grain size. The grain sizes of the MgO and Mg_2SiO_4 were calculated from the full width at half-maximum (FWHM) of diffraction peaks by the Suryanarayana and Grant Norton's formula [21] :

$$B_r(B_{crystalline} + B_{strain})\cos\theta = k\lambda/L + \eta\sin\theta \quad (1)$$

where B_r is the full width at half-maximum (FWHM) of the diffraction peak after instrumental correction; $B_{crystalline}$ and B_{strain} are the FWHM caused by a small grain size and internal stress, respectively; k is a constant (with a value of 0.9); λ is the wavelength of the X-ray radiation; L and η are the grain size and internal strain, respectively; and θ is the Bragg angle. The parameters B and B_r follow Cauchy's form with the relationship: $B = B_r + B_s$, where B and B_s are the FWHM of the broadened Bragg peaks and the standard sample's Bragg peaks, respectively.

The powders were placed in a graphite die (outside diameter, 45 mm; inside diameter, 20 mm; height, 40 mm) and then introduced into the High-frequency Induction Heating Sintering (HFIHS) apparatus shown schematically in references [17-20]. The HFIHS apparatus includes a 15 kW power supply which provides an induced current through the sample, and a 50 kN uniaxial press. The system was first evacuated and a uniaxial pressure of 80 MPa was applied. An induced current was then activated and maintained until the densification rate was negligible, as indicated by the real-time output of the shrinkage of the sample. The shrinkage was measured by a linear gauge measuring the vertical displacement. The HFIHS can be controlled in two ways: by temperature control or by output control. The latter was chosen to investigate the effect of the output of total power, given that the induced current level has a direct effect on the rate of heating and on the maximum temperature. The output level was 80% of the total power output. Temperatures were measured by a pyrometer focused on the surface of the graphite die. At the end of the process, the induced current was turned off and the sample cooled to room temperature. The process was carried out under a vacuum of 5.33 Pa.

The relative density of the sintered samples was measured by the Archimedes method. Microstructural information was obtained from product samples, which had been polished and etched using thermal etching for 1 h at 1200 °C. Compositional and microstructural analyses of the products were made through X-ray diffraction (XRD), field emission scanning electron microscopy (FE-SEM) with energy dispersive xray spectroscopy (EDS). Vickers hardness was measured by performing indentations at a load of 5 kg and a dwell time of 15 s.

Results and Discussion

Fig. 1 shows X-ray diffraction patterns of the MgO, MgO-10 wt%SiO_2, MgO-20 wt%SiO_2, MgO-30 wt%SiO_2, and MgO-40 wt%SiO_2 powders after high-energy ball milling for 4 h. Only MgO peaks are detected and SiO_2 peaks are not detected due to an amorphous phase. Fig. 2 shows plots of Brcosθ versus sinθ of MgO milled for 4 h to calculate particle sizes from XRD data. The average grain sizes of the MgO in milled MgO, MgO-10 wt%SiO_2, MgO-20 wt%SiO_2, MgO-30 wt%SiO_2, and MgO-40 wt%SiO_2 powders determined by Suryanarayana and Grant Norton's formula were about 20, 17, 15, and 17 nm, respectively.

FE-SEM images of MgO, MgO-10wt%SiO_2, MgO-20 wt%SiO_2, MgO-30 wt%SiO_2, and MgO-40 wt%SiO_2 powders after milling for 4 h are shown in Fig. 3. MgO and SiO_2 powders have a round shape, refined with milling

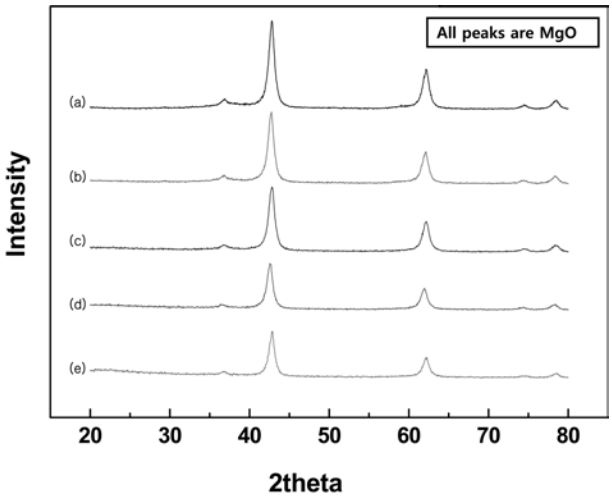

Fig. 1. X-ray diffraction patterns of the powder milled for 4 h; (a) MgO, (b) MgO-10 wt%SiO_2, (c) MgO-20 wt%SiO_2, (d) MgO-30 wt%SiO_2, and (e) MgO-40 wt%SiO_2.

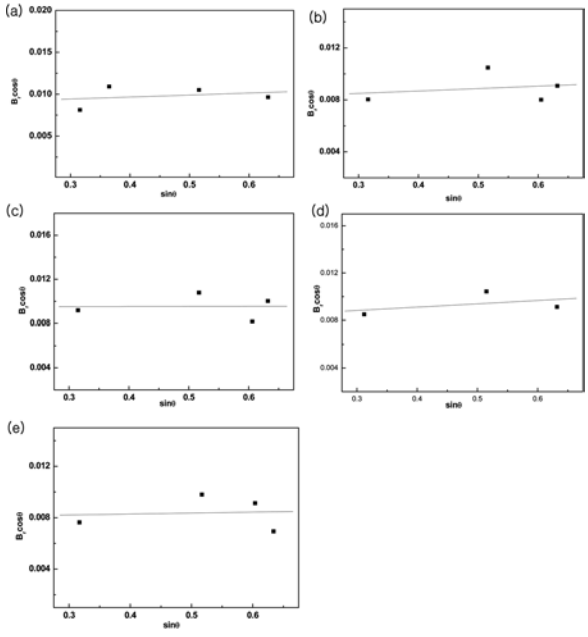

Fig. 2. Plot of B_r ($B_{crystalline}$ + B_{strain}) cosθ versus sinθ for the MgO powder milled for 4 h.

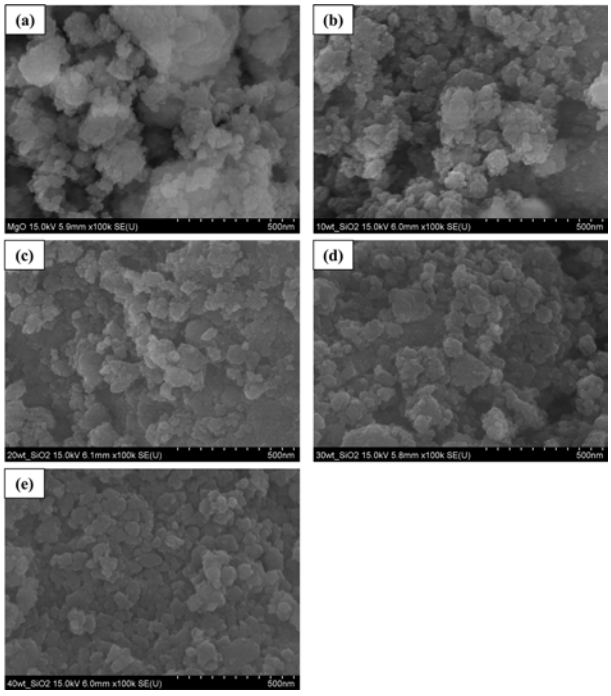

Fig. 3. FE-SEM images of the powder milled for 4 h; (a) MgO, (b) MgO-10 wt%SiO_2, (c) MgO-20 wt%SiO_2, (d) MgO-30 wt%SiO_2, and (e) MgO-40 wt%SiO_2.

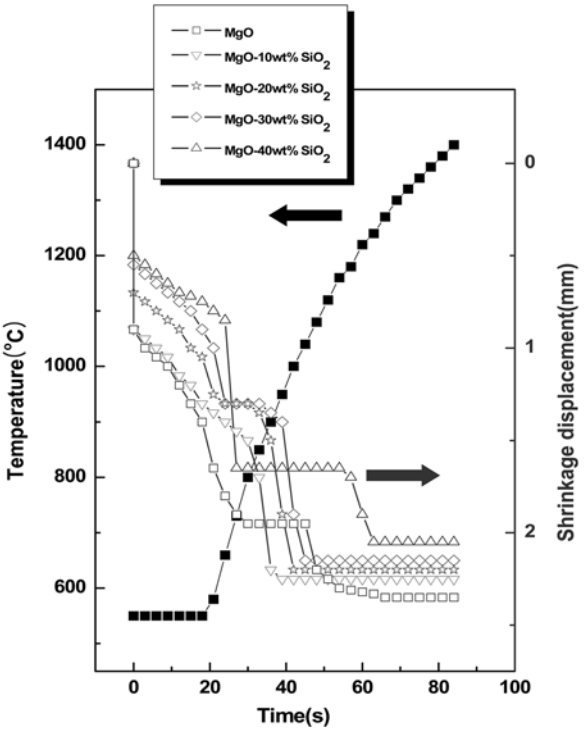

Fig. 4. Variations of temperature and shrinkage with heating time during the sintering of MgO-SiO_2 powders milled for 4 h.

and some agglomeration. The variations of the shrinkage displacement and temperature with the heating time for 80% of the total output power capacity (15 kW) during the sintering of the high energy ball milled MgO, MgO-10 wt%SiO_2, MgO-20 wt%SiO_2, MgO-30 wt%SiO_2, and

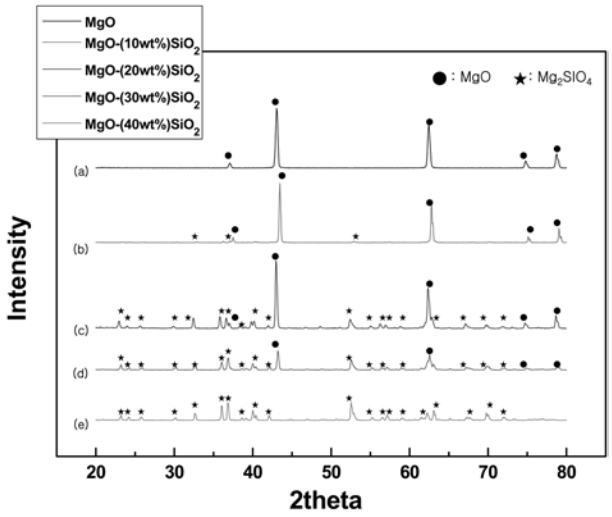

Fig. 5. X-ray diffraction patterns of the sintered specimens; (a) MgO, (b) MgO-10 wt%SiO_2, (c) MgO-20 wt%SiO_2, (d) MgO-30 wt%SiO_2, and (e) MgO-40 wt%SiO_2.

MgO-40 wt%SiO_2 powders under a pressure of 80 MPa are shown in Fig. 4. In all cases, the application of the induced current resulted in shrinkage due to consolidation. As the induced current was applied, the shrinkage continuously increased. Fig. 5 shows the XRD patterns of specimens sintered from the high energy ball milled MgO, MgO-10 wt%SiO_2, MgO-20 wt%SiO_2, MgO-30 wt%SiO_2, and MgO-40 wt%SiO_2 powders In Fig. 5(a) all peaks are MgO. And in case of the MgO-SiO_2 system, MgO and Mg_2SiO_4 peaks are detected. The interaction between these phases:

$$2MgO + SiO_2 \rightarrow Mg_2SiO_4 \quad (2)$$

is thermodynamically feasible [22].

Plots of B_r ($B_{crystalline} + B_{strain}$) cosθ versus sinθ of MgO and Mg_2SiO_4 in Suryanarayana and Grant Norton's formula [21] are shown in Fig. 6 and 7, respectively. The average grain sizes of the MgO and Mg_2SiO_4 in MgO, MgO-10 wt%SiO_2, MgO-20 wt%SiO_2, MgO-30 wt%SiO_2, and MgO-40 wt%SiO_2 systems calculated from the XRD data using Suryanarayana and Grant Norton's formula [21] were about 49, 68, 64, 103 nm and 94, 52, 53, 101 nm, respectively. The relative density of MgO sintered from milled powder MgO was 99%. Thus, the average grain size of the sintered MgO is not greatly larger than that of the initial powder, indicating the absence of much grain growth during sintering. This retention of the grain size is attributed to the high heating rate and the relatively short term exposure of the powders to the high temperature. FE-SEM images of MgO, MgO-Mg_2SiO_4 and Mg_2SiO_4 sintered from MgO, MgO-10 wt%SiO_2, MgO-20 wt%SiO_2, MgO-30 wt%SiO_2, and MgO-40 wt%SiO_2 powders milled for 4 h are shown in Fig. 8. MgO and Mg_2SiO_4 consist of nanocrystallites.

The role of the current (resistive or inductive) in sintering and or synthesis has been the focus of several attempts aimed

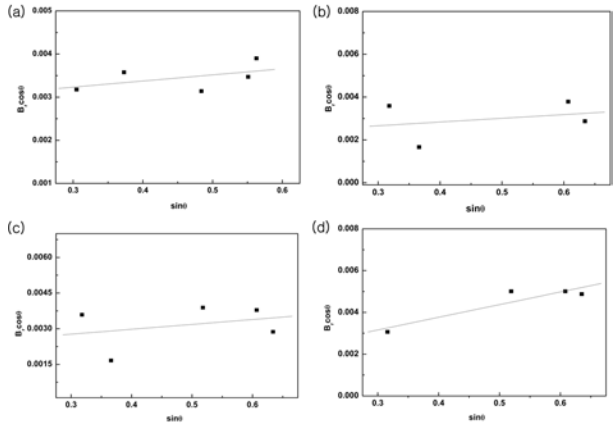

Fig. 6. Plot of B_r ($B_{crystalline} + B_{strain}$) cosθ versus sinθ for MgO sintered from various milled powders; (a) MgO, (b) MgO-10 wt%SiO_2, (c) MgO-20 wt%SiO_2, (d) MgO-30 wt%SiO_2, and (e) MgO-40 wt%SiO_2.

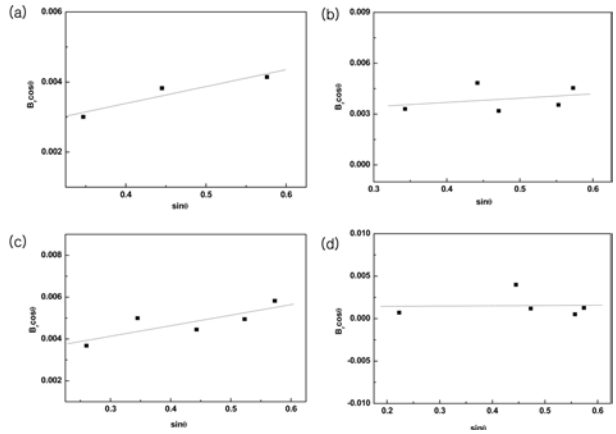

Fig. 7. Plot of B_r ($B_{crystalline} + B_{strain}$) cosθ versus sinθ for Mg_2SiO_4 sintered from various milled powders; (a) MgO-10 wt%SiO_2, (b) MgO-20 wt%SiO_2, (c) MgO-30 wt%SiO_2, and (d) MgO-40 wt%SiO_2.

at providing an explanation of the observed enhancement of sintering and the improved characteristics of the products. The role played by the current has been variously interpreted, the effect being explained in terms of a rapid heating rate due to Joule heating, the presence of a plasma in the pores separating the powder particles, and an intrinsic contribution of the current to mass transport [23-26].

Vickers hardness measurements were performed on polished sections of the MgO, MgO-Mg_2SiO_4 and Mg_2SiO_4 samples using a 5 kg load and 15 s dwell time. The Vickers hardnesses of MgO, MgO-Mg_2SiO_4 and Mg_2SiO_4 sintered from MgO, MgO-Mg_2SiO_4 and Mg_2SiO_4 sintered from MgO, MgO-10 wt%SiO_2, MgO-20 wt%SiO_2, MgO-30 wt%SiO_2, and MgO-40 wt%SiO_2 powders milled for 4 h were 540, 500, 400, 300 and 410 kg/mm^2, respectively. The hardnesses of MgO-Mg_2SiO_4 composites increased with an increase in MgO content. The fracture toughness could not be calculated from crack length because radial cracks did not emanate from the corners of the indent in all specimens. However, it is considered that the fracture

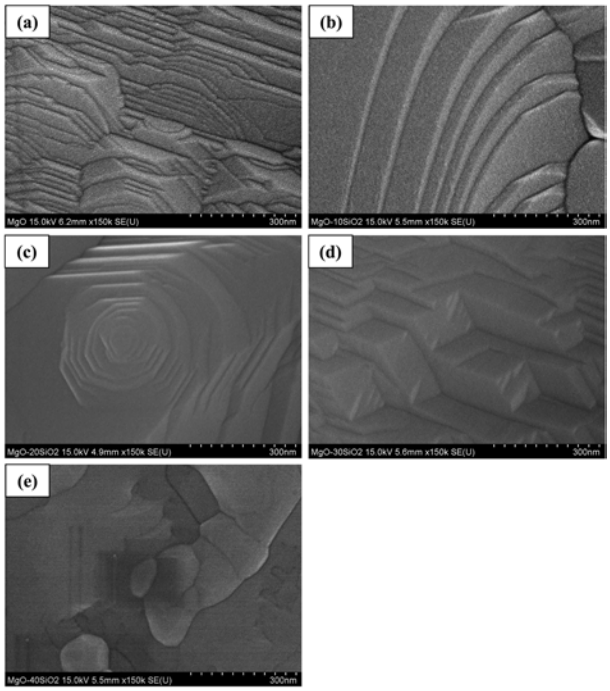

Fig. 8. FE-SEM images of sintered specimens ; (a) MgO, (b) MgO-10 wt%SiO_2, (c) MgO-20 wt%SiO_2, (d) MgO-30 wt%SiO_2, and (e) MgO-40 wt%SiO_2.

toughness of MgO-Mg_2SiO_4 composites is higher than that of Mg_2SiO_4 reported as 2.4 MPa.$M^{1/2}$ [10]. The absence of reported values for hardness and toughness of MgO-Mg_2SiO_4 precludes making a direct comparison to the results obtained in this study to show the influence of grain size.

Summary

Nanopowder of MgO was made using high-energy ball milling. Using the new rapid sintering method, HFIHS, the densification of MgO and MgO-Mg_2SiO_4 composites was accomplished using high energy ball milling. The average grain sizes of the MgO and Mg_2SiO_4 in MgO, MgO-10 wt%SiO_2, MgO-20 wt%SiO_2, MgO-30 wt%SiO_2, and MgO-40 wt%SiO_2 systems were about 49, 68, 64, 103 nm and 94, 52, 53, 101 nm, respectively. The relative density of MgO sintered from milled powder MgO was 99%. The Vickers hardnesses of MgO, MgO-Mg_2SiO_4 and Mg_2SiO_4 sintered from MgO, MgO-Mg_2SiO_4 and Mg_2SiO_4 sintered from MgO, MgO-10 wt%SiO_2, MgO-20 wt%SiO_2, MgO-30 wt%SiO_2, and MgO-40 wt%SiO_2 powders milled for 4 h were 540, 500, 400, 300 and 410 kg/mm^2, respectively.

Acknowledgment

"We are grateful for the financial support from the Korea Institute of Science and Technology, which was provided through the program for study on Development of Interfacial Engineering Technology Based on Plasma".

References

1. C. Vitale-Brovarone, S. Dinunzio, O. Bretcanu and E. Verne, J. Mater. Sci. Mater. Med. 15 (2004) 209-217.
2. C.T. Wu and J. Chang, Mater. Lett. 58 (2004) 2415-2417.
3. H.S. Ryu, K.S. Hong, J.K. Kim and J.H. Lee, Biomaterials 25 (2004) 393-401.
4. T.J. Webster, E.A. Massa-Schlueter, J.L. Smith and E.B. Slamovich, Biomaterials 25 (2004) 2111-2121.
5. K. Schwarz and D.B. Milne, Growth-promoting effects of silicon in rats, Nature 239 (1972) 333-334.
6. R.Z. LeGeros, Calcium Phosphates in Oral Biology and Medicine, Basel, Switzerland, 1991.
7. J.C. Dubois, C. Souchier, M.L. Couble, P. Exbrayat and M. LLissac, Biomaterials 20 (1999) 1841-1849.
8. D. Goeuriot, J.C. Dubois, d. Merle, F. Thevenot and P. Exbrayat, J. Eur. Ceram. Soc. 18 (1998) 2045-2056.
9. F. Tavangarian and R. Emadi, Synthesis of nanocrystalline forsterite (Mg_2SiO_4) powder by combined mechanical activation and thermal treatment, Materials Research Bulletin 45 (2010) 388-391.
10. Siyu Ni, Lee Chou and Jiang Chang, Ceramics International 33 (2007) 83-88.
11. M. Sherif El-Eskandarany, J. Alloys & Compounds 305 (2000) 225-238.
12. L. Fu, L.H. Cao and Y.S. Fan, Scripta Materialia 44 (2001) 1061-1068.
13. Z. Fang and J.W. Eason, Int. J. of Refractory Met. & Hard Mater 13 (1995) 297-303.
14. A.I.Y. Tok, L.H. Luo and F.Y.C. Boey, Matrials Science and Engineering A 383 (2004) 229-234.
15. I.J. Shon, D.K. Kim, I.Y. Ko, J.K. Yoon and K.T. Hong, Materials Science Forum 534-536 (2007) 525-528.
16. J. Jung and S. Kang, Scripta Materialia 56 (2007) 561-564.
17. H.C. Kim, D.Y. Oh, J. Guojian and I.J. Shon, Mater. Sci. Eng. A 368 (2004) 10-17.
18. H.C. Kim, D.Y. Oh and I.J. Shon, Int. J. Refract. Metals & Hard Mater. 22 (2004) 197-203.
19. D.Y. Oh, H.C. Kim, J.K. Yoon and I.J. Shon, J. Alloys & Compounds 386 (2005) 270-275.
20. H.C. Kim, D.Y. Oh and I.J. Shon, Int. J. Refract. Metals & Hard Mater. 22 (2004) 41-49
21. C. Suryanarayana and M. Grant Norton, X-ray Diffraction A Practical Approach, Plenum Press, New York, 1998.
22. O. Knacke, O. Kubaschewski and K. Hesselmann, Thermo-chemical Properties of Inorganic Substances, Springer-Verlag (1991).
23. Z. Shen, M. Johnsson, Z. Zhao and M. Nygren, J. Am. Ceram. Soc. 85 (2002) 1921-1927.
24. J.E. Garay, U. Anselmi-Tamburini, Z.A. Munir, S.C. Glade and P. Asoka- Kumar, Appl. Phys. Lett. 85 (2004) 573-575.
25. J.R. Friedman, J.E. Garay. U. Anselmi-Tamburini and Z.A. Munir, Intermetallics. 12 (2004) 589-597.
26. J.E. Garay, J.E. Garay. U. Anselmi-Tamburini and Z.A. Munir, Acta Mater., 51 (2003) 4487-4495.